PROTEINS
STRUCTURE ■ FUNCTION ■ BIOINFORMATICS

Regulatory mechanism of the light-activable allosteric switch LOV–TAP for the control of DNA binding: A computer simulation study

Emanuel Peter, Bernhard Dick, and Stephan A. Baeurle*

Department of Chemistry and Pharmacy, Institute of Physical and Theoretical Chemistry, University of Regensburg, Regensburg D-93040, Germany

ABSTRACT

The spatio-temporal control of gene expression is fundamental to elucidate cell proliferation and deregulation phenomena in living systems. Novel approaches based on light-sensitive multiprotein complexes have recently been devised, showing promising perspectives for the noninvasive and reversible modulation of the DNA-transcriptional activity *in vivo*. This has lately been demonstrated in a striking way through the generation of the artificial protein construct light-oxygen-voltage (LOV)–tryptophan-activated protein (TAP), in which the LOV-2-Jα photoswitch of phototropin1 from *Avena sativa* (AsLOV2-Jα) has been ligated to the tryptophan-repressor (TrpR) protein from *Escherichia coli*. Although tremendous progress has been achieved on the generation of such protein constructs, a detailed understanding of their functioning as opto-genetical tools is still in its infancy. Here, we elucidate the early stages of the light-induced regulatory mechanism of LOV–TAP at the molecular level, using the noninvasive molecular dynamics simulation technique. More specifically, we find that Cys450-FMN-adduct formation in the AsLOV2-Jα-binding pocket after photoexcitation induces the cleavage of the peripheral Jα-helix from the LOV core, causing a change of its polarity and electrostatic attraction of the photoswitch onto the DNA surface. This goes along with the flexibilization through unfolding of a hairpin-like helix-loop-helix region interlinking the AsLOV2-Jα- and TrpR-domains, ultimately enabling the condensation of LOV–TAP onto the DNA surface. By contrast, in the dark state the AsLOV2-Jα photoswitch remains inactive and exerts a repulsive electrostatic force on the DNA surface. This leads to a distortion of the hairpin region, which finally relieves its tension by causing the disruption of LOV–TAP from the DNA.

Proteins 2013; 81:394–405.

Key words: computer simulation of fusion proteins; LOV-based photoenzymes; light-regulated gene transcription; early signal transduction pathway; protein engineering.

INTRODUCTION

Gene expression in living systems is generally controlled by binding activator or repressor proteins to regulatory DNA sequences. The activity of transcription factors, on the other hand, is regulated at various levels, such as nuclear import, oligomerization, and DNA binding.[1] Chemical approaches enabling their modulation have encountered fast development in the past decades and are now widely used in biotechnological applications,[2–4] but they still often suffer from the drawback to be invasive and/or not rapidly reversible. Therefore, many efforts have recently been concentrated on developing fast reversible and noninvasive strategies for modulating gene expression *in vivo*. One possibility to reach these goals is to render gene expression light-controllable by ingeniously building photoswitches into any of the levels mentioned previously. An important example for light-mediated control of transcriptional activity by nuclear import and subsequent dimerization is the native photosystem composed of phytochrome and phytochrome-interacting factor (PIF), which regulates the growth of plants and microbes in response to red-light exposure. Photoconversion of phytochrome from its red-sensitive (Pr) to its far-red-sensitive (Pfr) form triggers a cryptic nuclear localization signal at its C-terminus, causing its import into the cell nucleus and association with PIFs.

Additional Supporting Information may be found in the online version of this article.

Grant sponsor: Deutsche Forschungsgemeinschaft (DFG) through the Research Training Group GRK 640 "Sensory photoreceptors in natural and artificial systems" as well as the Research Training Group GRK 1626 "Chemical photocatalysis."

*Correspondence to: Stephan A. Baeurle, Department of Chemistry and Pharmacy, Institute of Physical and Theoretical Chemistry, University of Regensburg, Regensburg D-93040, Germany. E-mail: stephan.baeurle@chemie.uni-regensburg.de
Received 16 May 2012; Revised 17 September 2012; Accepted 2 October 2012
Published online 8 October 2012 in Wiley Online Library (wileyonlinelibrary.com).
DOI: 10.1002/prot.24196

Shimizu-Sato *et al.*[5] demonstrated by fusing, respectively, the interacting modules of phytochrome B (phyB) and PIF3 to the DNA-binding and -activating domains of the yeast transcription factor GAL4 that the optical switching of the phyB-domain from the Pr- to the Pfr-conformer permits to regulate the transcriptional activity of GAL4. The system enabled the control of the extent of induction of gene expression in yeast through optical titration of the Pr/Pfr ratio, but it required an exogenous source of the tetrapyrrole chromophore phycocyanobilin. A similar process of light-induced dimerization between the sensor domain of plant cryptochrome 2 (CRY2) and its interacting partner cryptochrome-interacting basic helix-loop-helix protein 1 (CIB1) was evidenced by Liu *et al.*[6] to regulate the gene transcription in Arabidopsis cells. Moreover, Grossmann and coworkers[7] demonstrated that in the green algae *Chlamydomonas reinhardtii* the protein complex phototropin, which is composed of a serine/threonine kinase coupled to two N-terminal light-oxygen-voltage (LOV) sensitive domains designated as LOV1 and LOV2, is involved in the light-regulated expression of genes encoding chlorophyll and carotenoid biosynthesis enzymes. The LOV domains are flavin-based sensory proteins, which in the signaling state create a covalent linkage between the flavin-mononucleotide (FMN) and a nearby cysteine residue of the apoprotein. This induces conformational changes in the protein surrounding, which trigger a signal in the adjacent kinase. A similar route for light-mediated control of DNA-transcriptional activity was recently proposed by Strickland *et al.*,[8] which consists in fusing the tryptophan-repressor (TrpR) protein from the bacterium *Escherichia coli* with the AsLOV2-Jα domain from *Avena sativa*. This procedure enabled them to create a blue-light-activable allosteric switch, where a shared α-helix, the so-called Jα-helix, between both protein domains acts as a rigid lever arm regulating the affinity of the TrpR domain to the DNA. In this way, they were able to demonstrate that one of their construct, which they referred to as the LOV- and tryptophan-activated protein LOV–TAP, protects cognate DNA from digestion when illuminated. A similar native system with a LOV domain coupled to a helix-turn-helix DNA-binding protein (LOV–HTH) was recently isolated from the marine bacterium *Erythrobacter litoralis* and studied spectroscopically by Nash *et al.*[9] Although significant progress on the synthesis and structural characterization of such LOV-regulated DNA switches has already been accomplished, their structural-dynamical characteristics and functional behavior at the molecular level is still poorly understood.

To study the functional behavior of complex protein systems in nonequilibrium situations, we have recently introduced a novel noninvasive thermostating strategy, relying on the molecular dynamics (MD) algorithm,[10–12] and demonstrated its usefulness to explore the early stages of the switching mechanism of the AsLOV2-Jα photosensor at the molecular level. The so-called noninvasive MD technique permits to sample the protein's configurations far from equilibrium and to follow its natural dynamics under solvent-mediated thermostating control.[10] It has also lately successfully been used to elucidate the early signaling pathway of a LOV-regulated artificial photoenzyme, connecting the AsLOV2-Jα photosensor with a Rac1-GTPase,[13] and other isolated LOV domains, such as the LOV1 domain from the green algae *C. reinhardtii*[12] and the VIVID–LOV domain from the fungus *Neurospora crassa*.[14] The latter system is known to modulate the circadian clock of the fungus previously mentioned by regulating the levels of transcripts, encoded by the central clock gene frequency. Using our nonequilibrium MD technique, we could resolve the light-induced conformational changes, taking place after illumination of the VIVID monomer, and show that they play a major role in controlling the dimerization tendency of VIVID with its partner domains.

The goal of this article is to explore the regulatory mechanism of the artificial protein complex LOV–TAP at the molecular level, which enables the control of the DNA-binding affinity through light stimulation. To this end, we will use the noninvasive MD-simulation technique to investigate the early structural changes and functional behavior of its dark- and light-state form on the nanosecond timescale. Our study reveals that LOV–TAP in the light state is electrostatically attracted onto the DNA surface by unfolding the lever arm between the Jα-helix and the TrpR domain, whereas in the dark state this region remains rigid and permits the release of LOV–TAP from the DNA surface through electrostatic repulsion.

METHODS

Generation of starting structures

To create the starting model for our LOV–TAP simulations, we took the structures of the *E. coli* tryptophan-activated repressor (TAP; pdb-code: 1TRR)[15] and the AsLOV2-Jα photosensor (pdb-code: 2V0U),[16] determined by X-ray diffraction measurements, and generated the LOV–TAP dimer through connection of the AsLOV2-Jα system at Ala543 with the TAP structure at Phe22 on the chains D and E of TAP[8] (see Fig. 1). We then minimized the system in conjunction with the DNA using the l-BFGS minimizer and the GROMOS96-43a1 forcefield, to describe the interactions. Afterward, we centered the minimized structure in a cubic box with box-length of 14.9 nm and solvated the protein–DNA complex with simple point charge (SPC)-water molecules. We point out that, in addition to the LOV–TAP dimer complex, free TAP molecules were also attached onto the DNA. Finally, we neutralized the system by adding nine sodium ions and relaxed it in a short MD run of 0.5 ps with a timestep of 0.5 fs. During

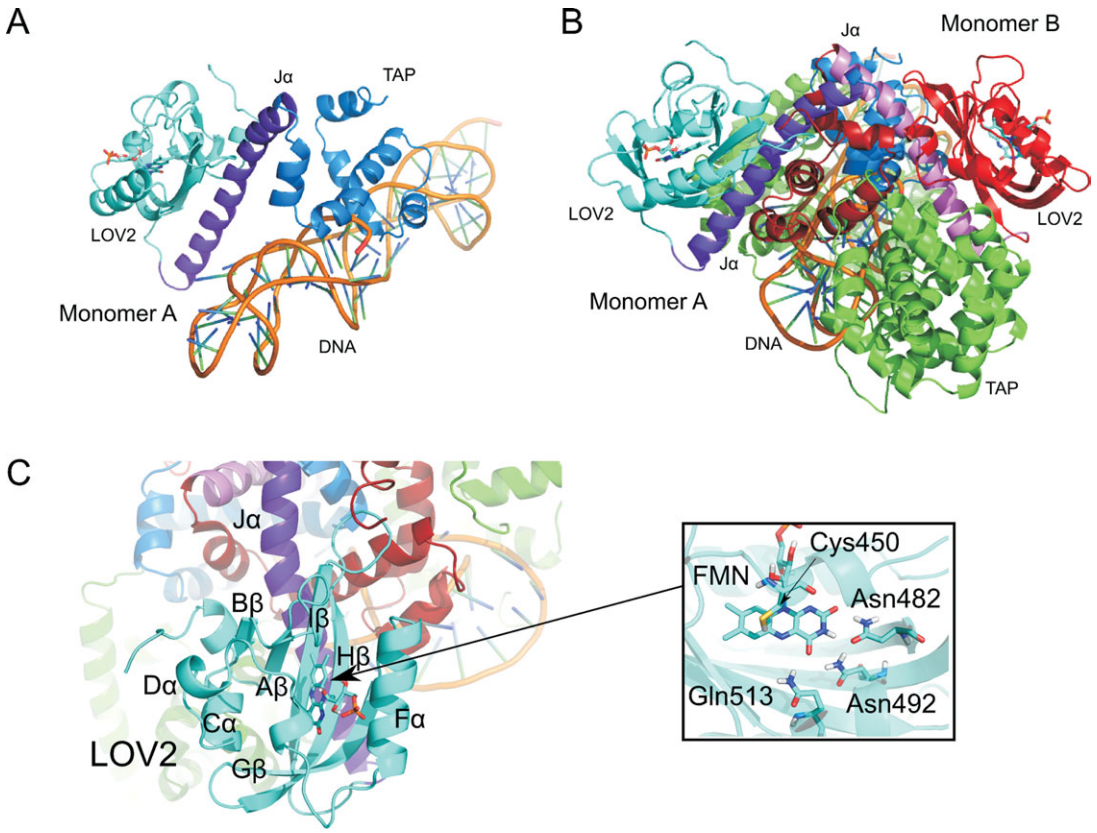

Figure 1

A: Tertiary structure of LOV–TAP monomer (monomer A) attached onto DNA. **B:** Tertiary structure of LOV–TAP dimer attached onto DNA (MD starting structure). **C:** Secondary structure elements of AsLOV2 domain with snapshot of amino-acid environment in vicinity to FMN chromophore [monomer A: AsLOV2 core (cyan), Jα-helix (violet), and TAP (blue); monomer B: AsLOV2 core (light red), Jα-helix (magenta), and TAP (dark red); and free TAP (green)].

this relaxation phase, a pressure of 1 atm and a temperature of 100 K were imposed using the Berendsen-thermostat and -barostat.[17] We validated our model through measurement of the radial-distribution function (RDF) and the radius of gyration of LOV–TAP in the dark-state form. Afterward, we compared the resulting data with the experiments of Strickland *et al.*[8] From Figure 1S, Supporting Information, we deduce that our LOV–TAP model possesses a maximum at 3.1 nm in the DNA–protein RDF, whereas the experimental RDF has a peak at 3.0 nm. Moreover, the radius of gyration of our model possesses an average value of 2.75 nm, whereas the experimentally determined radius of gyration has an average at 2.9 nm. From this analysis, we conclude that our model fits well to the experimental data of Strickland *et al.*, which validates it for further use in the MD simulations presented in the following. To create the initial structure for our light-state simulation, we used the model previously mentioned and generated a cysteinyl-FMN (CFN) adduct by forming a covalent bond between the Cys450-S and FMN-C4a. This covalent linkage between the reactive cysteine and FMN is required to transmit the stress from the reaction center to the protein surface and trigger the protein signal, as demonstrated in our previous MD-simulation studies with the AsLOV2-Jα-Rac1 photoenzyme[13] and the LOV1 domain from *C. reinhardtii*.[12]

Simulation details

To resolve the signal transduction pathway from LOV–TAP at the molecular level, we generated MD trajectories making use of the GROMACS MD simulation package version 4.0.3 in conjunction with the GROMOS96-43A1 forcefield[10,18] to describe the interactions. This widely used forcefield has been tested against NMR-spectroscopic data in case of the hen egg white globular protein lysozyme in water by Soares *et al.*[19] and has been found to reproduce its solution structure and conformational behavior very well. In a recent study, Todorova *et al.*[20] performed extensive MD simulations on the 51-amino-acid protein insulin and subjected the GROMOS96-43A1 forcefield to a systematic comparison against other popular biomolecular forcefields, including the CHARMM27, AMBER03, OPLS, and GROMOS96-53A6 forcefields. They analyzed in detail the effect of each forcefield on

the conformational evolution as well as structural properties of the protein and compared the results with the available experimental data. They observed that each forcefield favors different structural trends. Moreover, they found that the united-atom forcefield GROMOS96-43A1, together with the CHARMM27 forcefield, delivered the best description of the experimentally observed dynamic behavior of the chain B of insulin. In our simulations, we used in addition full particle-mesh-Ewald electrostatics with a Coulomb cutoff of 1.4 nm and computed the van der Waals interactions, using a shift function with a cutoff of 1.4 nm. To generate an isothermal–isobaric ensemble with a temperature of 300 K and a pressure of 1 atm, the system was equilibrated for 1 ns. During this phase, each part of the system was coupled to a Nosé–Hoover thermostat and a Parrinello–Rahman barostat.[17] We then performed a production run of 20 ns, in which the protein and FMN were decoupled from the thermostat, whereas the solvent and ions remained coupled. This procedure is known as the noninvasive thermostating technique, which allows the protein to sample configurations far from equilibrium and to follow its natural dynamics under solvent-mediated thermostating control.[10] For the numerical integration of the equations of motion, we used the leapfrog integrator with a timestep of 1 fs, while the neighbor list was updated every 10th step. To describe the interactions of the CFN, we used the parameters of Neiss and Saalfrank,[21] which were determined from B3LYP-6-31G*-calculation results and through comparison with similar groups in the forcefield to reach consistency. The reliability of the parametrization of the CFN and FMN was tested and confirmed by these authors on the LOV2 domain from *Adiantum capillus-veneris* without the Jα-helix[21] and by us on the AsLOV2-Jα system,[10] AsLOV2-Jα-Rac1 photoenzyme[13] as well as the LOV1 domain from *C. reinhardtii*.[11,12] To get an estimate of the binding free energy,[22] we assumed that under isothermal–isobaric conditions it can be expressed as

$$\Delta G_{\text{bind}} \approx \Delta U_{\text{bind}} - T\Delta S_{\text{bind}}, \qquad (1)$$

where ΔU_{bind} denotes the binding internal energy, while ΔS_{bind} and T represent the binding entropy and temperature of the system, respectively. We point out that in the previous formula we have discarded the contribution related to the volume change of the system $P\Delta V_{\text{bind}}$, because it is negligible for the process of dissociation of the protein–DNA complex in solution. To obtain an estimate for the binding internal energy, we used the following equation:

$$\Delta U_{\text{bind}} \approx \frac{1}{V}\int W(\mathbf{r})\mathrm{d}\mathbf{r} = -\frac{RT}{V}\int \ln g(\mathbf{r})\mathrm{d}\mathbf{r}, \qquad (2)$$

where $W(\mathbf{r})$ is the two-body potential of mean force (PMF) with $\mathbf{r}$ as the relative position between protein and DNA, whereas $g(\mathbf{r})$ and R designate the radial pair distribution function and universal gas constant, respectively. We note that the PMF represents the average work needed to bring the protein and DNA from infinite separation to a distance, $|\mathbf{r}|$,[23] and takes into account all related intrinsic interactions as well as solvent effects.[24] An approximation of the binding entropy is obtained by using[25]

$$\Delta S_{\text{bind}} \approx -\frac{1}{2}k_{\text{B}}\rho N_{\text{A}}\int [g(\mathbf{r})\ \ln\ g(\mathbf{r}) - g(\mathbf{r}) + 1]\ \mathrm{d}\mathbf{r} \qquad (3)$$

with N_{A} and ρ as Avogadro's number and density, respectively. Moreover, we emphasize that similar expressions based on a PMF have already successfully been used in investigations of protein–ligand binding.[26] Finally, we point out that we have analyzed the electrostatic surfaces of all states of LOV–TAP with the adaptive Poisson–Boltzmann solver (APBS).[27]

RESULTS AND DISCUSSION

We start the analysis of our simulation results by considering the spatio-dynamical behavior of characteristic amino acids in vicinity to the FMN chromophore in case of the dark and light states. In Figure 2(A), we show the dihedral angle, enclosing the atoms Gln513-(CA-CB-CD-OE1) of the Gln513 side chain, as a function of simulation time. For the light state, we observe an abrupt jump in the average angle from −150 up to 100° in the time range from 7500 to 12,000 ps. By comparing this result to the light-state curve for the interatomic distance between the atoms Gln513-OE1 and Asn492-ND2 in Figure 2(B), we infer that the change in the dihedral angle correlates with the drop of the latter quantity to H-bond distance at a simulation time of 12,000 ps, leading to a dramatic reduction of the magnitude of the fluctuation. By contrast, in case of the dark state, it stabilizes around an average value of 4.6 Å after 5000 ps by retaining a larger fluctuation amplitude compared to the light state. From these observations, we conclude that the side-chain rotation of Gln513 in the light state leads to a coupling between Gln513 and Asn492 through H-bond formation, whereas in the dark state no H-bond formation takes place between these residues. These findings are confirmed by considering the initial and final configurations of the amino acids surrounding the FMN chromophore in the light state in the Figure 2(C,D), respectively. In this context, it is worth pointing out that the glutamine residue adjacent to the FMN chromophore is highly conserved in all LOV domains in their native form and has previously been suggested to play a major role at the onset of their signaling pathway.[10] For example, some early experimental studies on the isolated LOV2 domain suggested that the primary process after CFN-adduct formation involves the breakage of a H-bond between

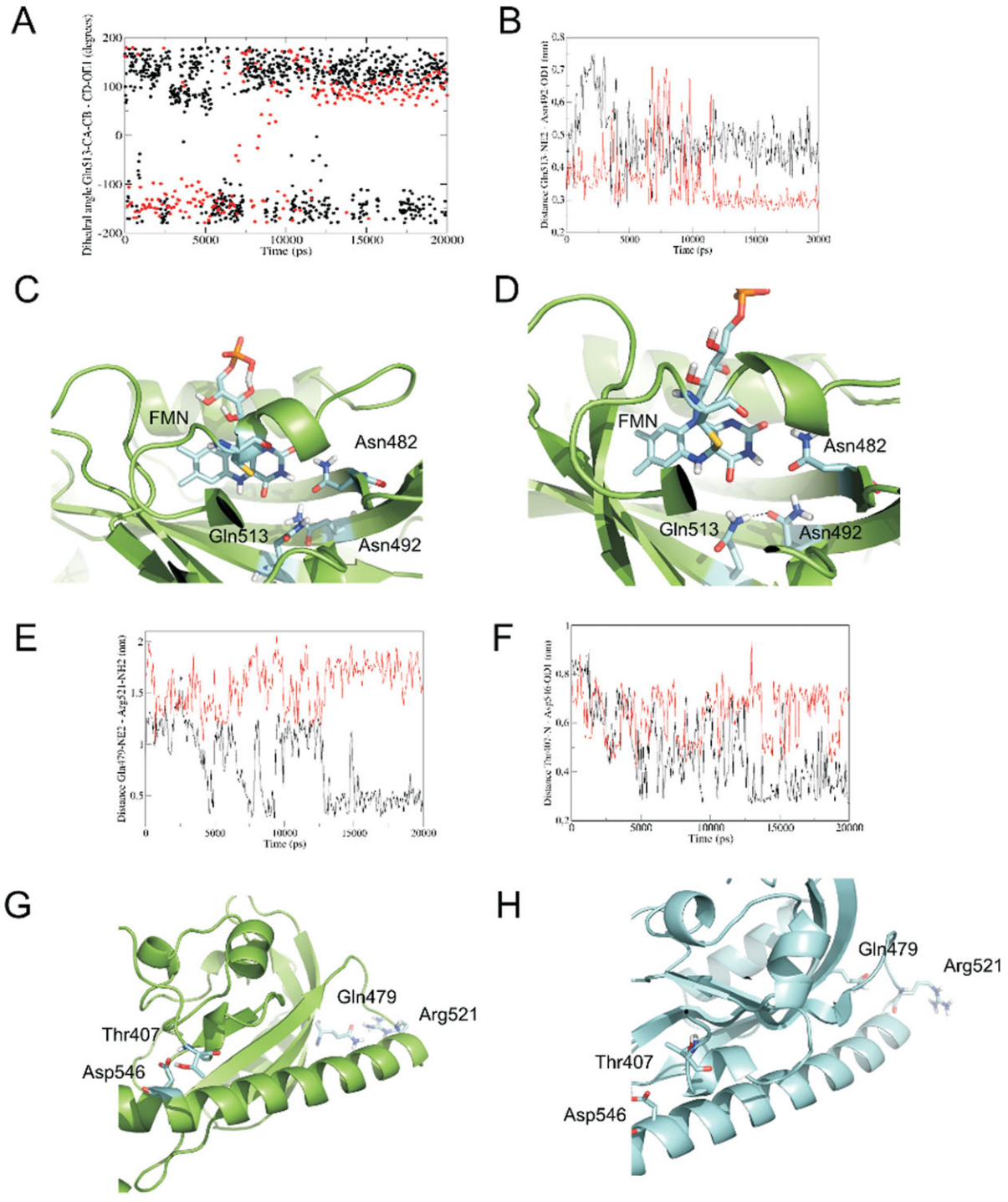

Figure 2

Dihedral angle or distances of characteristic atoms from amino acids surrounding the FMN chromophore of the dark (black) and light (red) states of LOV–TAP as a function of simulation time [**A:** dihedral angle Gln513-(CA-CB-CD-OE1) and **B:** distance Gln513-NE2–Asn492-OD1]. Local configurations of amino acids Gln513, Asn492, and Asn482 surrounding the FMN chromophore of the light state at the start (**C**) and end (**D**) of the simulation [cyan: C-atom; red: O-atom; blue: N-atom; white: H-atom; orange: P-atom; and yellow: S-atom]. Interatomic distances at AsLOV2-Jα interface of the dark (black) and light (red) states of LOV–TAP as a function of simulation time [**E:** Gln479-NE2–Arg521-NH2 and **F:** Thr407-N–Asp546-OD1]. Final configurations of secondary structural elements with characteristic amino acids at the AsLOV2-Jα interface [**G:** dark state and **H:** light state]. [Color figure can be viewed in the online issue, which is available at wileyonlinelibrary.com.]

the glutamine residue and the FMN-O4,[28] possibly followed through rotation of its side chain by the formation of a new H-bond with the FMN-N5.[29,30] In a later crystallographic study on the AsLOV2-Jα system, Halavaty and Moffat[16] proposed a local reorientation of the conserved glutamine, associated with a disruption of a H-bond between an asparagine and aspartic acid on the surface of the protein. In a series of spectroscopical investigations with point mutations on the LOV2-Jα system,[31,32] as well as the full-length phototropin,[33] it was demonstrated that this glutamine residue plays a central role in both spectral tuning and propagating the signal via the Iβ-strand from the LOV core to the Jα-helix, while its lack attenuates light-induced autophosphorylation of the phototropin. In recent simulation studies on the isolated AsLOV2-Jα photoswitch[10] as well as the artificial photoenzyme AsLOV2-Jα-Rac1-GTPase,[13] we have demonstrated that the coupling process between Gln513 and Asn492, located on the Iβ- and Hβ-strands, respectively, triggers the disruption of the Jα-helix in the light state. Moreover, we showed that this process leads to a stabilization of the smaller β-strands at the outer peripheral part of the LOV2 domain known as the Aβ- and Bβ-strands,[10] which is in agreement with the low-temperature FTIR and UV–visible spectroscopic experiments of Iwata *et al.*[34] This causes a tightening of the β-sheet and contributes to an increase in the hydrophobicity of the LOV2 domain at the interface, which accelerates the detachment of the Jα-helix from the LOV2 domain. In the following, we will analyze the effect of this tightening process on the AsLOV2-Jα interface of LOV–TAP by considering the interatomic distances and configurations of amino acids residing at the N- and C-terminal parts of the Jα-helix. In Figure 2(E), we visualize the interatomic distances between the atoms Gln479-NE2 and Arg521-NH2, which are located on the Gβ-strand of the AsLOV2 domain in vicinity to the N-terminal part of the Jα-helix. We observe that the light-state curve undergoes a stable fluctuation around an average value of about 1.5 nm, whereas the dark-state curve performs a first drop to H-bond distance at around 5000 ps and after an intermediate range of large fluctuation amplitude stabilizes to H-bond distance after 15,000 ps. Similar conclusions can be drawn from the interatomic distances between the atoms Thr407-N and Asp546-OD1, shown in Figure 2(F). These latter residues are located at the N-terminal A′α-helix of the AsLOV2 domain and the C-terminal region of the Jα-helix. We note that the initial drop to H-bond distance of the dark-state curves of both interatomic distances Gln479-NE2 and Arg521-NH2 as well as Thr407-N and Asp546-OD1 in the N- and C-terminal parts of the AsLOV2-Jα interface correlates with the stabilization of the dark-state curve of the interatomic distance between Gln513-OE1 and Asn492-ND2 near to the N-terminal region of the Jα-helix at the same simulation time. From this observation, we deduce that in the dark state, where no coupling between the Hβ- and Iβ-strands takes place, the N-terminal region of the AsLOV2-Jα interface is stabilized, leading to an improved binding of the Jα-helix on the β-sheet of the AsLOV2 domain. By contrast, we find that in the light state, the H-bond formation between Gln513-OE1 and Asn492-ND2 leads to a stabilization of the tightened β-sheet conformation of the AsLOV2 domain, which indicates that this process is crucial for the disruption of H-bonds in the N-terminal part of the AsLOV2-Jα interface. Next, we show representative configurations of the AsLOV2-Jα interface in the final simulation stage for the dark and light states in Figure 2(G,H), respectively. From these figures, we conclude that the residues Asp546 and Thr407 in the C-terminal part of the Jα-helix as well as the residues Gln479 and Arg521 in the N-terminal part of the Jα-helix are H-bonded in the dark state, whereas they are disrupted in the light state. This confirms that the Jα-helix is cleaved from the AsLOV2 core in the light state, whereas it is stabilized on the surface of the β-sheet in the dark state. We point out that a similar photoswitching mechanism is observed in case of the AsLOV2-Jα system in the second monomer, as shown in Figure 2S, Supporting Information. Finally, we note that the possibility that the disruption of the Jα-helix might be the critical event in the signaling pathway has first been proposed by Harper *et al.* in their seminal study on the AsLOV2-Jα photoswitch.[10,35] To show this, they compared the dark- and CFN-adduct state 3D-HNCO-spectra of the isolated AsLOV2-Jα system, using the minimum chemical-shift-difference method to quantify the spectral changes. They observed within the LOV2 core large differences for the residues close to the FMN chromophore as well as for the ones on the Gβ-, Hβ-, and Iβ-strands. Significant perturbations were also found at sites on the Eα-helix and Jα-helix over 15 Å away from the FMN chromophore. They concluded from their work that the stresses resulting from the structural rearrangements, induced by the formation of the CFN adduct, propagate through the LOV domain, ultimately causing the disruption of the Jα-helix. Finally, we emphasize that a similar photoswitching mechanism, as found in case of the LOV–TAP system discussed herein, has also been observed in our previous simulation studies with the AsLOV2-Jα-Rac1-GTPase[13] as well as on the isolated AsLOV2-Jα system.[10] However, in the former case, the main events are to some extent shifted in their spatio-temporal behavior with regard to the other AsLOV2-regulated systems, due to the presence of the TrpR domain and the DNA. It is also worth noting in this context that this mechanism is in opposition to the mechanism recently proposed by Zayner *et al.*,[36] who suggested based on mutational analysis, circular dichroism (CD) and NMR experiments that the role of the β-sheet in the undocking process of the Jα-helix can be neglected and a N-terminal A′α-helix is the decisive control element for the light-activated con-

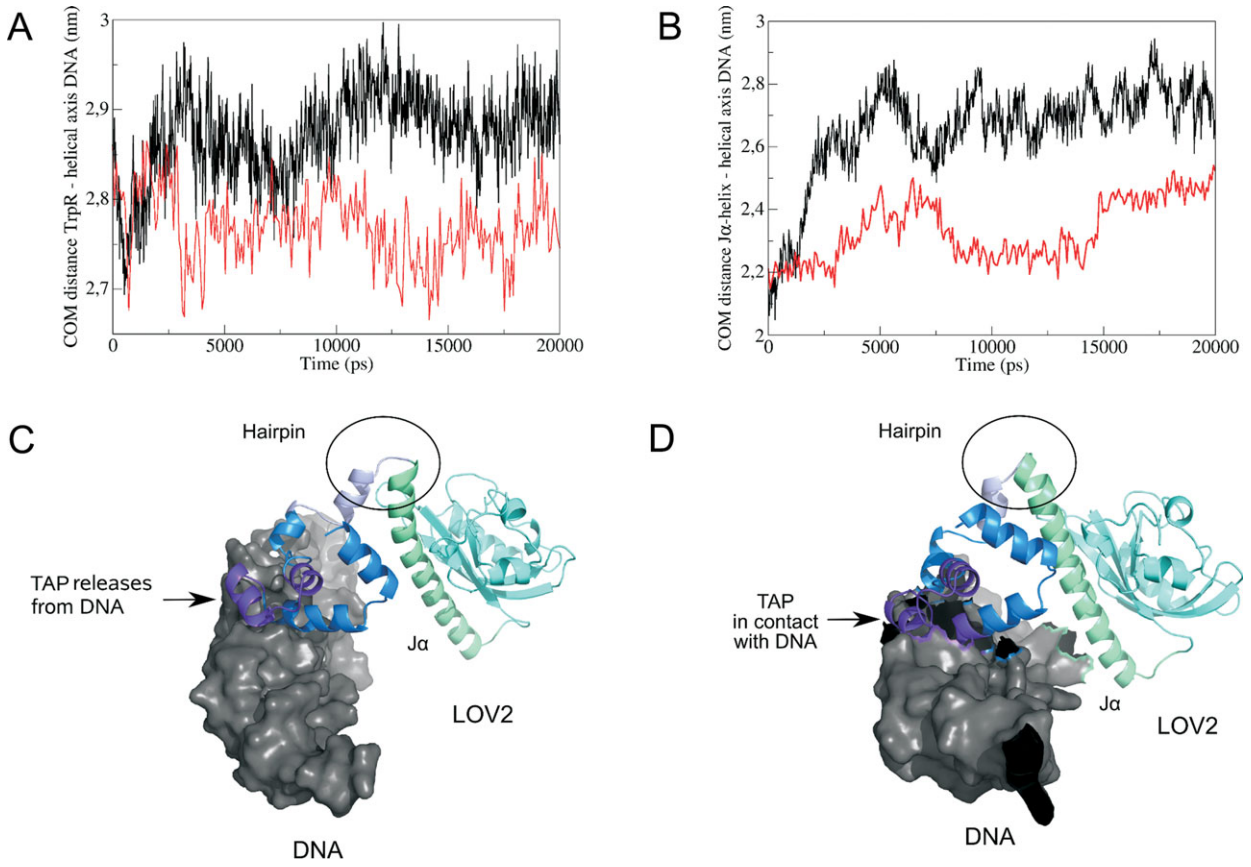

Figure 3

Distances between the COMs of characteristic structural elements from LOV–TAP at the LOV–TAP–DNA interface and the helical axis of DNA in the dark (black) and light (red) states of LOV–TAP as a function of simulation time [**A:** COM distance between TrpR and helical axis of DNA and **B:** COM distance between Jα helix and helical axis of DNA]. In addition, we show the final structures of a LOV–TAP monomer from the dimer in the dark-state (**C**) or light-state (**D**) form [AsLOV2 core (cyan); hairpin: Jα-helix (light green); N-terminal part of repressor (light violet); TAP part not in contact with DNA in light state (blue); TAP part in contact with DNA in light state (dark violet); and DNA (gray)]. [Color figure can be viewed in the online issue, which is available at wileyonlinelibrary.com.]

formational changes in the AsLOV2 domain, instead. To test their proposal, they made single-point mutations either on the C-terminal or on the N-terminal part of the AsLOV2-Jα interface but still observed the light-activated conformational changes attributed to the disruption of the Jα-helix in their CD spectrum. These experiments show that both the N-terminal and the C-terminal parts of the AsLOV2-Jα interface contribute to the disruption of the Jα-helix in the isolated AsLOV2-Jα domain, which is confirmed by our simulation results[10,37] and the experiments of Harper *et al.*[35,38] as well as of Nash *et al.*[31] Finally, we emphasize that the structural-dynamical changes observed in the AsLOV2-Jα photosensor in case of the dark-state simulation are likely to be induced by the covalently linked TAP–DNA complex and might be of importance for the functional behavior of LOV–TAP in the dark.

In the following, we study in more detail the structural-dynamical changes taking place at the interface between LOV–TAP and the DNA in the LOV–TAP–DNA complex upon photoactivation and elucidate the implication of the photoswitching mechanism in the AsLOV2-Jα system in controlling the binding affinity of LOV–TAP to the DNA surface. To this end, we first consider in Figure 3(A) the distances of the center-of-mass (COM) between the TrpR and the helical axis of the DNA from LOV–TAP in the dark and light states. Although both curves possess a similar initial behavior up to 2500 ps, the dark-state curve continues to grow drastically up to 3000 ps and then performs a stable fluctuation with an amplitude of 0.1 nm about an average distance of 2.9 nm. By contrast, in the same time period, the light-state curve decreases and undergoes a stable fluctuation about an average distance of 2.75 nm with similar amplitude. The average difference in distance between the dark and light states therefore amounts to 0.15 nm, which indicates that the TrpR is released from the DNA in the dark state, whereas it binds to it in the light state. To elucidate the

mechanism of activation, we visualize next in Figure 3(B) the distances of the COM between the Jα-helix of the AsLOV2 domain and the helical axis of the DNA from LOV–TAP in the dark and light states. We find that, after an initial increase of the quantity up to a maximum value of 2.8 nm attained at a simulation time of 5000 ps, the dark-state curve undergoes a stable fluctuation around an average distance of 2.7 nm up to the end of the simulation run. By contrast, in case of the light state the curve increases only slightly and performs a stable fluctuation around an average distance of 2.3 nm with a magnitude of about 0.1 nm. By comparing these results with the ones of the interatomic distances between Gln479-NE2 and Arg521-NH2 in Figure 2(E), we note that the upshift in the dark-state curve, taking place from the onset of the simulation up to 5000 ps, correlates with the successive drop to H-bond distance of the dark-state curve of the latter quantity. This indicates that the photoswitching mechanism in the AsLOV2-Jα system is affected by the binding process between LOV–TAP and the DNA and may be involved in controlling the DNA-binding affinity. To further analyze the structural-dynamical changes involved in the DNA-binding process of LOV–TAP, we consider in the following in the Figure 3(C,D) the final structures of a single LOV–TAP monomer in the dark and light states, respectively, obtained after 20 ns of MD simulation. From the light-state structure, we conclude that the TrpR domain binds to the DNA surface by forming molecular contacts and that this binding process is induced by the condensation of the AsLOV2-Jα photoswitch onto the DNA surface. In case of the dark-state structure, we observe that the TrpR domain releases from the DNA surface, which goes along with the disruption of the AsLOV2-Jα photoswitch from the DNA and the simultaneous restitution of its N-terminal part through H-bond formation. These findings are confirmed through the distances between the COMs of the TrpR domain as well as the Jα-helix and the DNA-helical axis, shown in the Figure 3(A,B) respectively. To further investigate the light-induced changes in the binding affinity of the LOV–TAP–DNA complex from an energetic point of view, we show next in Figure 4(A,B) the binding free energies between the TrpR domain and DNA as well as the Jα-helix and DNA in the dark and light states as a function of simulation time, respectively. We conclude from both dark-state curves that the binding free energy between the two protein entities and the DNA increases over the course of the simulation run, which demonstrates that the binding strength of the molecular contacts decreases at the LOV–TAP–DNA interface in the dark state. By contrast, from the light-state curves, we deduce that the quantity remains nearly constant by fluctuating about an average value of −77 kJ/mol in case of the TrpR-DNA complex and −26 kJ/mol in case of the Jα-helix-DNA complex throughout the whole simulation run. This indicates that stable molecular contacts are formed during the simulation in case of LOV–TAP in the light state. Moreover, by comparing our theoretically estimated values for the binding free energy of the TrpR–DNA complex to the experimental results for the same system, that is, −53.48 kJ/mol,[39] as well as for the repressor-DNA complex from phage434, that is, −43.11 kJ/mol,[40] we infer that our theoretical results for the binding free energy are in reasonable agreement with the experimental measurements. Thus, we conclude from these findings that the photoswitching mechanism in the AsLOV2-Jα system controls the binding affinity of LOV–TAP to the DNA through varying the binding strength between LOV–TAP and the DNA surface.

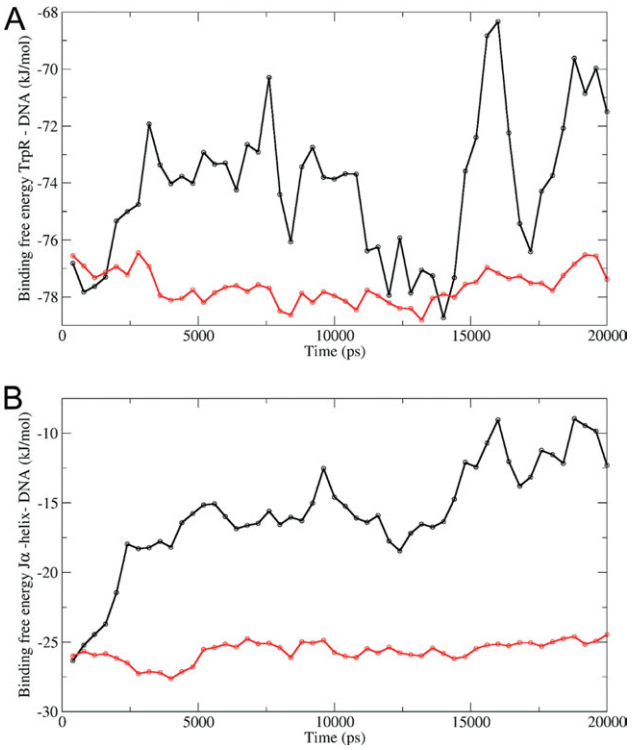

Figure 4

Binding free energies between (**A**) TrpR domain and DNA as well as (**B**) Jα-helix and DNA within the LOV–TAP–DNA complex in the dark (black) and light (red) states as a function of simulation time. [Color figure can be viewed in the online issue, which is available at wileyonlinelibrary.com.]

In the subsequent part, we study the conformational changes taking place in the region between the C-terminal end of the Jα-helix and the N-terminal part of the TrpR domain in the range of residues spanning from 549 to 559, which is a piece of the so-called hairpin region. To this end, we consider in Figure 5(A,B) the secondary structure analyses from LOV–TAP in the dark and light states, respectively. We observe that in the hairpin region α-helical unfolding occurs in case of the light state at a simulation time of 12,000 ps, which correlates with the H-bond formation process taking place between residues

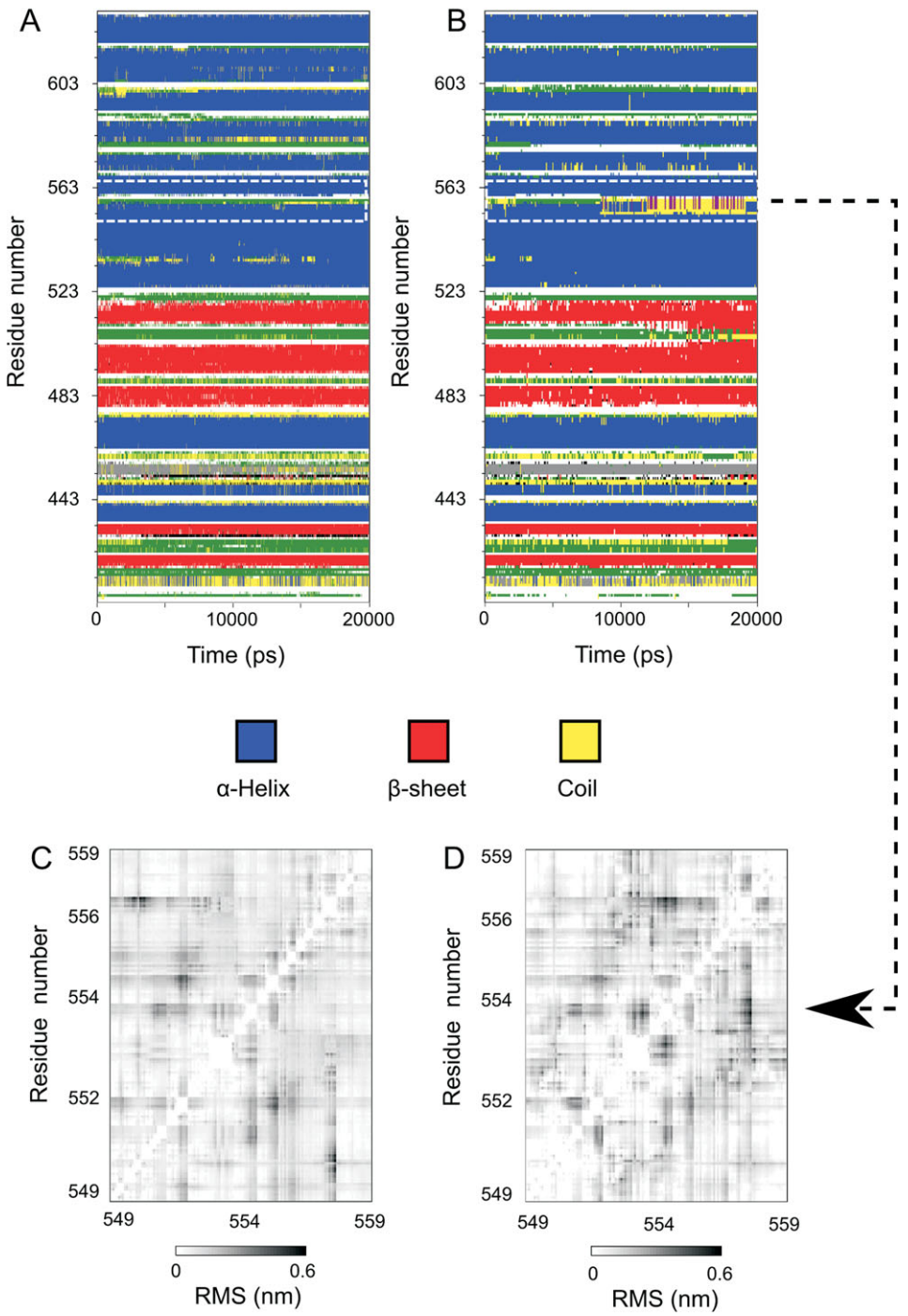

Figure 5

Secondary-structure analyses from simulations of LOV–TAP in the dark-state (**A**) or light-state (**B**) form. RMS-distance matrix from simulations of LOV–TAP in the dark-state (**C**) or light-state (**D**) form. [Color figure can be viewed in the online issue, which is available at wileyonlinelibrary.com.]

Asn492 and Gln513 on the Hβ- and Iβ-strands [see Fig. 2(B)]. By contrast, we notice that in the dark state the hairpin region remains folded throughout the whole simulation run. From these findings, we conclude that in the light state the β-sheet tightening process of the AsLOV2 domain as well as the subsequent cleavage of the Jα-helix leads to the α-helical unfolding in the hairpin region, which in turn affects the amino acids at the TrpR-DNA interface. Next, in Figure 5(C,D), we analyze the hairpin region through considering the root-mean-square (RMS)

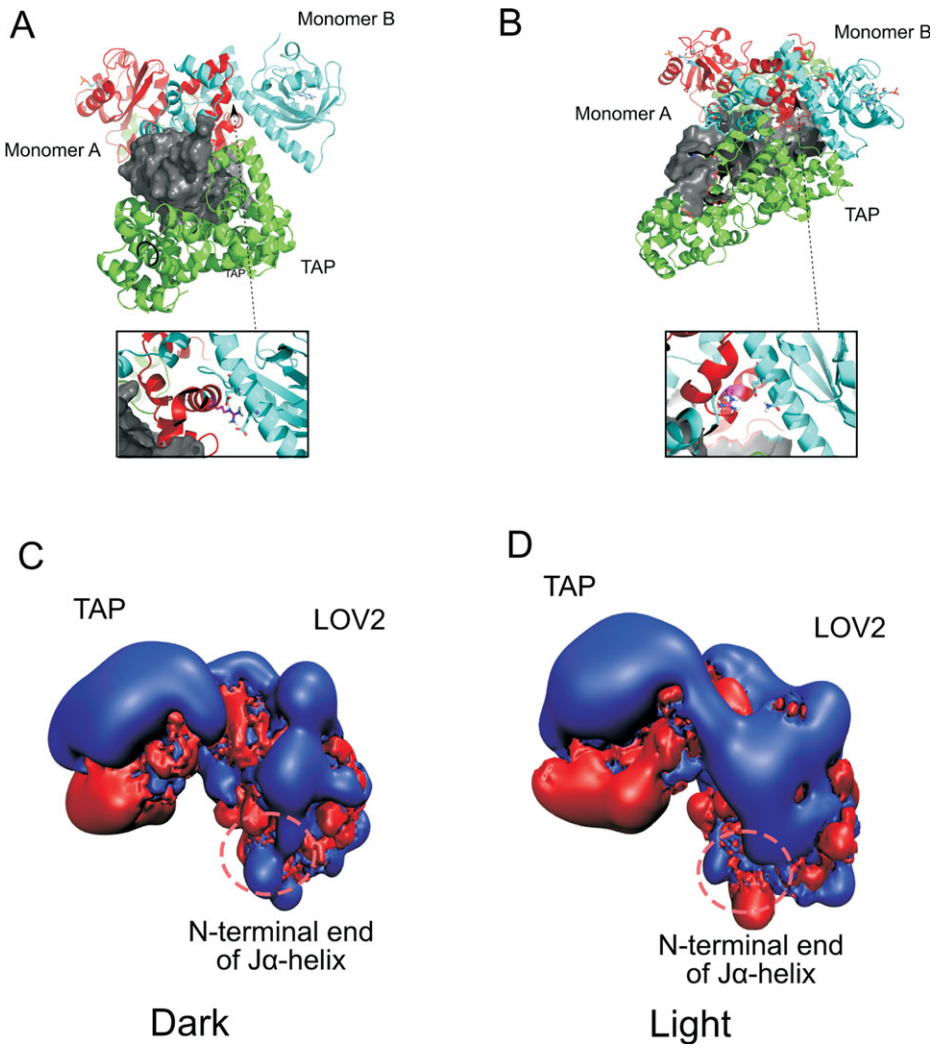

Figure 6

Final structures of the LOV–TAP–DNA dimer in the dark-state (**A**) or light-state (**B**) form with snapshot of LOV–TAP–DNA binding site at the interface between the Jα-helix of LOV–TAP and the DNA [monomer A (red), monomer B (cyan), free TAP (green), DNA (gray)]. In addition, we display the APBS-electrostatic surfaces of a LOV–TAP monomer from the dimer in the dark-state (**C**) or light-state (**D**) form. Note that the orientations of the surfaces correspond to the final structures of the LOV–TAP monomer in the dark (C) and light (D) states, shown in the Figure 3(C,D) respectively. Moreover, the red and blue colors designate electrostatic charge magnitudes of $+2k_BT/e$ and $-2k_BT/e$, respectively. [Color figure can be viewed in the online issue, which is available at wileyonlinelibrary.com.]

deviation as a function of the residue number in the dark and light states, respectively. We observe that the RMS matrix of the light state possesses large RMS values of about 0.6 nm in the residue ranges 552–554 and 555–557, whereas in the dark state it adopts much smaller values in these regions. Therefore, our analysis shows that the hairpin region has an overall larger flexibility in the light state, due to the unfolding process taking place in the residue range 549–559, and indicates that the increased mobility of this lever arm from LOV–TAP enables the TrpR domain to bind onto the DNA. In this context, it is worth mentioning that the mechanism of TrpR binding has been experimentally investigated by several authors in *E. coli*. For example, Lawson and Carey[15] and Otwinowski *et al.*[41] determined, through X-ray-diffraction measurements, the structural affinity of the TrpR domain for binding onto the DNA and elucidated the role of the corepressor tryptophan (Trp). The latter molecule is known to adhere tightly onto the TrpR domain, which causes its tilting and binding to the DNA.[42] We note that LOV–TAP in its dark-state form mimics the state in which Trp is missing in the native system, resulting in the detachment of the TrpR domain from the DNA. To further demonstrate that our simulation approach can be used to investigate the binding mechanism of the LOV–TAP dimer, we visualize in Figure 6(A,B) the final overall structures of the LOV–TAP dimer with snapshots of the interface between the Jα-helix of LOV–TAP and the DNA

in the dark and lights states, respectively. In addition, we consider in Figure 3(C,D) for both states the final structures of a single LOV–TAP monomer by focusing on the hairpin region, encompassing the Jα-helix and N-terminal part of TAP, as well as the TAP protein part, adhering onto the DNA surface. We deduce from the dark-state dimer as well as the monomer structures that both LOV–TAP monomers are released from the DNA, while in case of the corresponding light-state structures we find that both LOV–TAP monomers bind onto the DNA surface. Moreover, we infer from the APBS-electrostatic surface of the dark-state monomer, displayed in Figure 6(C), that the AsLOV2-Jα system possesses a strong negative charge concentration at the N-terminal end of the Jα-helix. This leads to its electrostatic repulsion from the negatively charged DNA surface, inducing a bending force and subsequent distortion of the stiffly folded hairpin region [see Fig. 3(C)]. To relieve this tension in the hairpin region, the TrpR–DNA interface is cleaved and the LOV–TAP successively detaches from the DNA surface, ultimately leading after full equilibration to the functionally active dark-state configuration. In this state, the DNA is freely accessible for DNA transcription or nuclease digestion. We note that, to attain this final equilibrium dark-state configuration, further investigations will be necessary using novel multiscale modeling techniques, which enable to extend the range of accessible timescales far beyond the nanosecond timescale.[37] By contrast, from the APBS-electrostatic surface of the light-state monomer, shown in Figure 6(D), we deduce that the N-terminal end of the Jα-helix adopts a positive charge, induced by the CFN-adduct formation in the AsLOV2 core and subsequent detachment of the Jα-helix. This leads to an electrostatic attraction of the AsLOV2-Jα photoswitch onto the DNA, resulting in the unfolding and subsequent flexibilization of the hairpin region [see Fig. 5(B)]. This ultimately leads to the condensation of TAP onto the DNA surface. In this state, DNA transcription or nuclease digestion is inhibited in agreement with the experimental observations of Strickland *et al.*[8]

CONCLUSIONS

In summary, in this work, we have elucidated the regulatory mechanism of the light-activable DNA-binding switch LOV–TAP at a molecular level, using the noninvasive MD technique. Our study demonstrates in particular that the initial processes after formation of the Cys450-FMN adduct in the AsLOV2-Jα photoswitch upon photoexcitation involve the coupling between the amino acids Gln513 and Asn492 through H-bond formation in vicinity of the FMN chromophore, causing a change in polarity and electrostatic attraction of the photoswitch onto the DNA surface. This goes along with the flexibilization through unfolding of a hairpin-like helix-loop-helix region interlinking the AsLOV2-Jα- and TrpR-domains, ultimately enabling the condensation of LOV–TAP onto the DNA surface. By contrast, in the inactive dark state, the Jα-helix remains attached to the LOV2 core, and the photoswitch exerts a repulsive electrostatic force on the DNA surface, leading to a distortion of the stiffly folded hairpin region. To relieve the tension, the TrpR-DNA interface is cleaved successively, ultimately causing the release of LOV–TAP from the DNA. By further comparing these results to experimental observations, we conclude that our noninvasive simulation technique provides reliable information about the system at molecular resolution. Moreover, we find that it can be a useful complementary tool to elucidate as well as optimize functional behavior of complex proteins in opto-genetical applications.

REFERENCES

1. Liu L, White MJ, MacRae TH. Transcription factors and their genes in higher plants. Eur J Biochem 1999;262:247–257.
2. Gatz C. Chemical control of gene expression. Annu Rev Plant Physiol Plant Mol Biol 1997;48:89–108.
3. Gottesfeld JM, Turner JM, Dervan PB. Chemical approaches to control gene expression. Gene Expr 2000;9:77–91.
4. Padidam M. Chemically regulated gene expression in plants. Curr Opin Plant Biol 2003;6:169–177.
5. Shimizu-Sato S, Huq E, Tepperman JM, Quail PH. A light-switchable gene promoter system. Nat Biotechnol 2002;20:1041–1044.
6. Liu H, Yu X, Li K, Klejnot J, Yang H, Lisiero D, Lin C. Photoexcited CRY2 interacts with CIB1 to regulate transcription and floral initiation in *Arabidopsis*. Science 2008;322:1535–1539.
7. Im C-S, Eberhard S, Huang K, Beck CF, Grossmann AR. Phototropin involvement in the expression of genes encoding chlorophyll and carotenoid biosynthesis enzymes and LHC apoproteins in *Chlamydomonas reinhardtii*. Plant J 2006;48:1–16.
8. Strickland D, Moffat K, Sosnick TR. Light-activated DNA binding in a designed allosteric protein. Proc Natl Acad Sci USA 2008;105:10709–10714.
9. Nash AI, McNulty R, Shillito ME, Swartz TE, Bogomolni RA, Luecke H, Gardner KH. Structural basis of photosensitivity in a bacterial light-oxygen-voltage/helix-turn-helix (LOV–HTH) DNA-binding protein. Proc Natl Acad Sci USA 2011;108:9449–9454.
10. Peter E, Dick B, Baeurle SA. Mechanism of signal transduction of the LOV2-Jα-photosensor from *Avena sativa*. Nat Commun 2010;1:122.
11. Peter E, Dick B, Baeurle SA. Effect of computational methodology on the conformational dynamics of the protein photosensor LOV1 from *Chlamydomonas reinhardtii*. J Chem Biol 2011;4:167–184.
12. Peter E, Dick B, Baeurle SA. Signals of LOV1: a computer simulation study on the wildtype LOV1-domain of *Chlamydomonas reinhardtii* and its mutants. J Mol Model 2012;18:1375–1388.
13. Peter E, Dick B, Baeurle SA. Signaling pathway of a photoactivable Rac1-GTPase in the early stages. Proteins: Struct Funct Bioinform 2012;80:1350–1362.
14. Peter E, Dick B, Baeurle SA. Illuminating the early signaling pathway of a fungal light-oxygen-voltage photoreceptor. Proteins: Struct Funct Bioinform 2012;80:471–481.
15. Lawson CL, Carey J. Tandem binding in crystals of a trp repressor/operator half-site complex. Nature 1993;366:178–182.
16. Halavaty AS, Moffat K. N- and C-terminal flanking regions modulate light-induced signal transduction in the LOV2 domain of the blue light sensor phototropin 1 from *Avena sativa*. Biochemistry 2007;46:14001–14009.

17. Frenkel D, Smit B. Understanding molecular simulation: from algorithms to applications. San Diego: Academic Press; 2003.
18. Lindahl E, Hess B, van der Spoel D. GROMACS 3.0: a package for molecular simulation and trajectory analysis. J Mol Model 2001;7:306–317.
19. Soares T, Daura X, Oostenbrink C, Smith L, Gunsteren W. Validation of the GROMOS force-field parameters set 45A3 against nuclear magnetic resonance data of hen egg lysozyme. J Biomol NMR 2004;30:407–422.
20. Todorova N, Legge FS, Treutlein H, Yarovsky I. Systematic comparison of empirical forcefields for molecular dynamic simulation of insulin. J Phys Chem B 2008;112:11137–11146.
21. Neiss C, Saalfrank P. Molecular dynamics simulation of the LOV2 domain from *Adiantum capillus-veneris*. J Chem Inf Comput Sci 2004;44:1788–1793.
22. Gohlke H, Klebe G. Approaches to the description and prediction of the binding affinity of small-molecule ligands to macromolecular receptors. Angew Chem Int Ed 2002;41:2644–2676.
23. Chandler D. Introduction to modern statistical mechanics. New York: Oxford University Press; 1987.
24. Leach AR. Molecular modelling: principles and applications. Essex: Pearson Education; 2001.
25. Lazaridis T. Inhomogeneous fluid approach to solvation thermodynamics. 1. Theory. J Phys Chem B 1998;102:3531–3541.
26. Mitchell JBO, Laskowski RA, Alex A, Thornton JM. BLEEP-potential of mean force describing protein–ligand interactions: I. Generating potential. J Comput Chem 1999;20,1165–1176; and references therein.
27. Baker NA, Sept D, Joseph S, Holst MJ, McCammon JA. Electrostatics of nanosystems: application to microtubules and the ribosome. Proc Natl Acad Sci USA 2001;98:10037–10041.
28. Nozaki D, Iwata T, Ishikawa T, Todo T, Tokutomi S, Kandori H. Role of Gln1029 in the photoactivation processes of the LOV2 domain in *Adiantum* Phytochrome3. Biochemistry 2004;43:8373–8379.
29. Crosson S, Moffat K. Photoexcited structure of a plant photoreceptor domain reveals a light-driven molecular switch. Plant Cell 2002;14:1067–1075.
30. Fedorov R, Schlichting I, Hartmann E, Domratcheva T, Fuhrmann M, Hegemann P. Crystal structures and molecular mechanism of a light-induced signaling switch: the phot-LOV1 domain from *Chlamydomonas reinhardtii*. Biophys J 2003;84:2474–2482.
31. Nash AI, Ko W-H, Harper SM, Gardner KH. A conserved glutamine plays a central role in LOV domain signal transmission and its duration. Biochemistry 2008;47:13842–13849.
32. Yamamoto A, Iwata T, Sato Y, Matsuoka D, Tokutomi S, Kandori H. Light signal transduction pathway from flavin chromophore to the Jα helix of *Arabidopsis* phototropin 1. Biophys J 2009;96:2771–2778.
33. Jones MA, Feeney KA, Kelly SM, Christie JM. Mutational analysis of phototropin 1 provides insights into the mechanism underlying LOV2 signal transmission. J Biol Chem 2007;282:6405–6414.
34. Iwata T, Nozaki D, Tokutomi S, Kagawa T, Wada M, Kandori H. Light-induced structural changes in the LOV2 domain of *Adiantum* Phytochrome3 studied by low-temperature FTIR and UV–visible spectroscopy. Biochemistry 2003;42:8183–8191.
35. Harper SM, Neil LC, Gardner KH. Structural basis of a phototropin light switch. Science 2003;301:1541–1544.
36. Zayner JP, Antoniou C, Sosnick TR. The amino-terminal helix modulates light-activated conformational changes in AsLOV2. J Mol Biol 2012;419:61–74.
37. Peter E, Dick B, Baeurle SA. A novel computer simulation method for simulating the multiscale transduction dynamics of signal proteins. J Chem Phys 2012;136:124112.
38. Harper SM, Christie JM, Gardner KH. Disruption of the LOV–Jα helix interaction activates phototropin kinase activity. Biochemistry 2004;43:16184–16192.
39. Carey J. Trp repressor arms contribute binding energy without occupying unique locations on DNA. J Biol Chem 1989;264:1941–1945.
40. Brown LM, Bruccoleri RE, Novotny J. Empirical free energy calculations of phage 434 repressor- and cro-DNA complexes support the 'indirect readout' hypothesis of specificity. Pac Symp Biocomput 1998;339–348.
41. Otwinowski Z, Schevitz RW, Zhang R-G, Lawson CL, Joachimiak A, Marmorstein RQ, Luisi BF, Sigler PB. Crystal structure of trp repressor/operator complex at atomic resolution. Nature 1988;335:321–329.
42. Alberts B, Johnson A, Lewis J, Raff M, Roberts K, Walter P. Molecular biology of the cell. New York: Garland Science; 2008.